ACS OMEGA

Open Access

http://pubs.acs.org/journal/acsodf

Article

Glassy Fluorene and Sulfone Polyesters with High Refractive Index and Thermal Stability Whose Monomers Induce Estrogenic Bioactivity

Gavin S. Mohammad-Pour, Aditya Maan, Rachel Kemp, Thomas J. Kean,* and Kaitlyn E. Crawford*

Cite This: *ACS Omega* 2025, 10, 9613−9622

Read Online

ACCESS | Metrics & More | Article Recommendations | Supporting Information

ABSTRACT: Two new diacid monomers containing either fluorene or sulfone moieties polymerize via step-growth polymerization in the presence of their diol counterparts or alkyl diols (ethylene glycol and 1,6-hexanediol), forming eight new *cardo* structure polyesters. The polymers exhibit high optical transparency in the thin-film form with refractive indices ranging from 1.56 to 1.69, tunable glass transition temperatures from ca. 40 to 116 °C with no melting temperature, and resistance to thermal degradation in a nitrogenous atmosphere, reaching 350−398 °C before observing 10% weight loss. Their molecular weights, M_w, range from ca. 17 to 77 kDa, with an average polydispersity, $Đ$, of 1.5, and average purified yields of 82%. The polymers absorb light primarily in the UV region from ca. 228 to 320 nm with no absorption from 320 to 800 nm. A critical finding is that some of the fluorene and sulfone monomers induce negative bioactivity and even cell death in T47D-KBLuc cells, a breast cancer cell line, at high concentrations. This report details the project inspiration, monomer synthesis, polymerization steps, structural confirmation, material characterization, and the impact of the new monomer's estrogenic and antiestrogenic bioactivity.

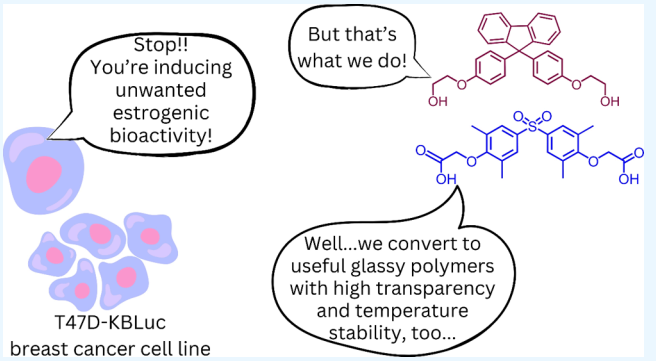

1. INTRODUCTION

Fluorene- and sulfone-based polymers, particularly those with *cardo* structures, are drawing attention for their wide-ranging use in applications from optics,[1,2] electronics,[3,4] and sensing,[5,6] to antistatic coatings[7,8] and medical supplies.[9,10] The broad use of fluorene-based polymers (FBPs) and sulfone-based polymers (SBPs) stems from their distinctive polymer properties like high refractive index, permeability, thermal stability, and low birefringence.[11−13] Fluorene and sulfone polyarylates have been known for some time, primarily from the step-growth polymerization between bisphenols and acid chlorides or carboxylic acids.[14−20] As a result of FBP's and SBP's promising multipurpose properties, exploration of fluorene and sulfone monomer derivatives is expanding,[21,22] and translational studies involving FBPs and SBPs are increasing.[23,24] While FBP and SBP materials remain interesting for advanced technology applications, their monomers can exhibit negative bioactivity owing to their similar chemical shape to hormones, just like the well-known endocrine disrupter bisphenol A (BPA); Figure 1. For example, compounds such as bisphenol-S (BPS), bisphenol-F (BPF), and fluorene-9-bisphenol (BHPF), sometimes used as substitutes for BPA in commercial products, are themselves endocrine disruptors.[25−28] The alarming negative bioactivity of some FBP and SBP monomers highlights concerns like deciding when a material's beneficial properties for advancing technologies do not outweigh its potentially negative biological impact and to what extent the use of starting materials like BPS, BPF, and BHPF ought to be regulated in consumer products. In the meantime, identifying new fluorene and sulfone monomers with chemical architectures unique from those of hormones without losing the properties that make BHPF and SBP materials useful could offer a workaround solution. Hormones like estrogens are critical for controlling the growth, development, and homeostasis of many tissues in humans and mammals.[29,30] Estrogenic (and antiestrogenic) bioactivity can be evaluated using the T47D-KBLuc cell line, which was developed in 2004 to screen chemicals for estrogenic/antiestrogenic activity.[31] The T47D-KBLuc cell line has been used to identify estrogenic activity in BPA derivatives,[32] and its use in this work identifies the estrogenic/antiestrogenic bioactivity of two monomers, 2,2′-(((9*H*-fluorene-9,9-diyl)bis(4,1-phenylene))bis(ethan-1-ol) (F-diol)

Received: November 30, 2024
Revised: February 5, 2025
Accepted: February 10, 2025
Published: February 28, 2025

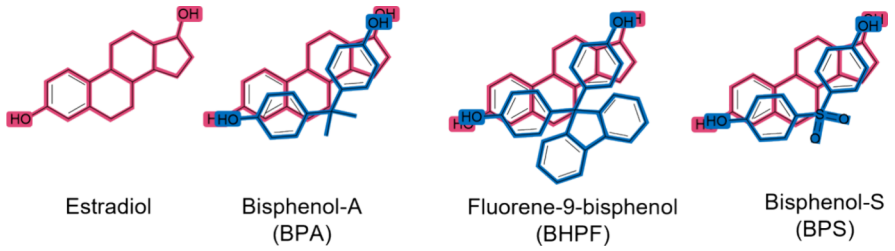

Figure 1. Estrogen hormone, estradiol (pink). Endocrine disruptors, BPA, BHPF, and BPS (blue), overlaid on estradiol.[25−28]

Scheme 1. Synthesis of Monomers[a]

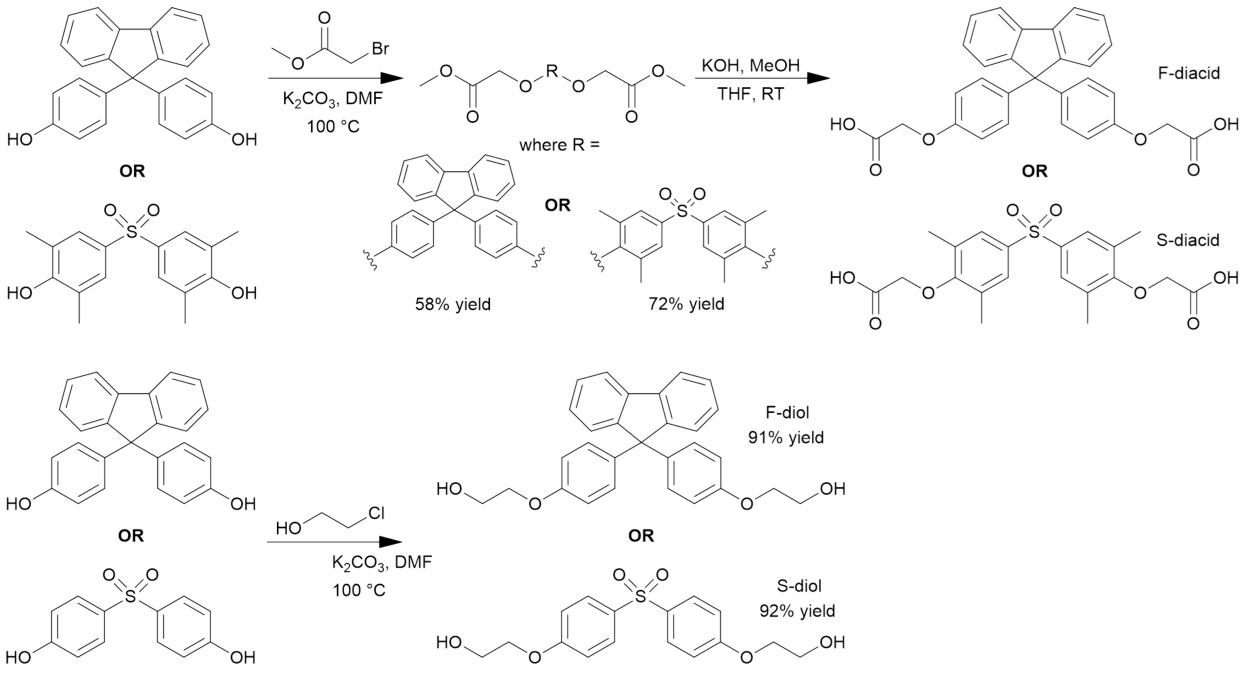

[a]Top: F-diacid and S-diacid. Bottom: F-diol and S-diol.

and 2,2′-((sulfonylbis(2,6-dimethyl-4,1-phenylene))bis(oxy))-diacetic acid (S-diacid). Here, we modified the BPF and BPS monomer structures by extending the terminal functional groups (alcohols or acids) away from the aromatic moieties with the aim of producing polymers whose monomers exhibit less endocrine-disrupting bioactivity without losing the high optical transparency and thermal properties of the BHPF and BPS polymers. In the proceeding sections, we describe the process of synthesizing the two new diacid monomers containing either fluorene or sulfone moieties, demonstrate their use in step-growth polymerization to achieve polymers with excellent optical and thermal properties, and report on their estrogenic/antiestrogenic bioactivity.

2. MATERIALS AND METHODS

2.1. Chemicals and Reagents. Solvents and starting materials, including monomers 1,6-hexanediol and 1,2-ethanediol, were purchased from commercial vendors (Fisher and Sigma-Aldrich). All materials were used as received, unless otherwise noted. Solvents were purified by using a solvent purification system (Innovative Technology). Standard organic transformation reactions were used to synthesize the fluorene and sulfone monomers. The synthetic steps are detailed in the Supporting Information (SI) and are accompanied by ^{1}H and ^{13}C NMR spectra (Figures S1−S4); brief descriptions of monomer and polymer synthesis steps follow below.

2.2. Synthesis. *2.2.1. Dicarboxylic Acid Fluorene Monomer (F-Diacid).* The **F-diacid** monomer described here has been reported for the first time. Monomer synthesis was achieved in two steps, according to Scheme 1. First, Williamson Ether synthesis was employed to couple 4,4′-(9*H*-fluorene-9,9-diyl)diphenol (BHPF) with bromomethyl acetate ($CH_3CO_2CH_2Br$; 2 eq with slight excess) in the presence of potassium carbonate (K_2CO_3) in dimethylformamide (DMF) at 100 °C for 24 h, resulting in the formation of dimethyl-2,2′-(((9*H*-fluorene-9,9-diyl)bis(4,1-phenylene))bis(oxy))diacetate (**F-precursor**; 72% yield). Second, complete hydrolysis of the **F-precursor** was achieved in the presence of potassium hydroxide (KOH) and a mixture of methanol (MeOH) and tetrahydrofuran (THF) at room temperature, resulting in the formation of the **F-diacid** monomer, 2,2′-(((9*H*-fluorene-9,9-diyl)bis(4,1-phenylene))bis(oxy))diacetic acid.

2.2.2. Dicarboxylic Acid Sulfone Monomer (S-Diacid). The S-diacid monomer described here has been reported for the first time. Monomer synthesis was achieved in two steps according to Scheme 1. First, Williamson Ether synthesis was employed to couple sulfonylbis(2,6-dimethylphenol) (SDMP) with $CH_3CO_2CH_2Br$ (2 eq with slight excess) in the presence

https://doi.org/10.1021/acsomega.4c10782
ACS Omega 2025, 10, 9613−9622

of K_2CO_3 in DMF at 100 °C for 24 h, resulting in the formation of dimethyl-2,2′-((sulfonylbis(2,6-dimethyl-4,1-phenylene))bis(oxy))diacetate (**S-precursor**; 58% yield). Second, complete hydrolysis of the **S-precursor** was achieved in the presence of KOH and a mixture of MeOH and THF at room temperature, resulting in the formation of the **S-diacid** monomer, 2,2′-((sulfonylbis(2,6-dimethyl-4,1-phenylene))bis-(oxy))diacetic acid. The average S-precursor yield was 58%, and hydrolysis to form the S-diacid was complete.

2.2.3. Diol Fluorene Monomer (F-Diol). The **F-diol** monomer was synthesized based on previous reports.[33,34] Monomer synthesis was achieved in one step according to Scheme 1. Williamson Ether synthesis was employed to couple BHPF with chloroethanol ($Cl(CH_2)_2OH$; 2 eq with slight excess) in the presence of K_2CO_3 in DMF at 100 °C, resulting in the formation of the **F-diol** monomer, 2,2′-(((9*H*-fluorene-9,9-diyl)bis(4,1-phenylene))bis(ethan-1-ol); average yield, 91% (∼9 g).

2.2.4. Diol Sulfone Monomer (S-Diol). The **S-diol** monomer was synthesized based on previous reports.[33,34] Monomer synthesis was achieved in one step, according to Scheme 1. Williamson Ether synthesis was employed to couple 4,4′-sulfonyldiphenol with $Cl(CH_2)_2OH$ (2 eq. with slight excess) in the presence of K_2CO_3 in DMF at 100 °C, resulting in the formation of the **S-diol** monomer, 2,2′-((sulfonylbis-(4,1-phenylene))bis(oxy))bis(ethan-1-ol); average yield, 92% (∼6 g).

2.2.5. Generalized Carbodiimide Polymerization Procedure. Selected diacid and diol monomers were reacted in an inert atmosphere with dimethylamine pyridinium tosylate (DPTS) (1:1:0.4 equiv) with anhydrous dichloromethane at 0 °C followed by the dropwise addition of *N*,*N*′-diisopropylcarbodiimide (DIC; 2.2 equiv) before heating at 45 °C for 48 h. The reactions were cooled to room temperature, then quenched in methanol (MeOH), and allowed to stir for 12 h before filtering, washing in MeOH, and drying under high vacuum at ∼60 °C.

2.3. Characterization Techniques. *2.3.1. Spectroscopy.* Nuclear magnetic resonance (NMR; Bruker AVANCE-III 400 MHz) spectroscopy was used to record ^1H and ^{13}C spectra of the monomers and polymers in DMSO-d_6 or $CDCl_3$ at room temperature with tetramethylsilane as an internal reference. Gas chromatography-mass spectroscopy (GC-MS; Agilent 7820 GC coupled with a 5977E MSD) was used to analyze the monomers. Monomer samples were prepared in HPLC-grade acetone (Sigma-Aldrich >99.9%, used as received) at 200 ppm concentrations. The GC column (Agilent DB-5ht) was made of polyimide with dimensions of 30 m × 250 and 0.25 μm internal silica coating. Helium was used as the carrier gas at a flow rate of 1.2 mL/min, and the oven's temperature program was as follows: 50 °C for 2 min, followed by a 20 °C/min ramp to 350 °C, and was then held at 350 °C for 3 min. Splitless injection was used with an injection volume of 1 μL and an injector temperature of 325 °C. The injection syringe was rinsed with HPLC-grade acetone ×3 prior to each sample injection. MS peaks were analyzed with an MS software database (MassHunter 7.0). Attenuated total reflectance-Fourier transform infrared spectroscopy (ATR-FTIR; JASCO 6600) was used to record IR spectra (16 scans) of the monomers and polymers in the powder form from 500 to 4000 cm^{-1} wavenumbers. UV−vis spectroscopy (UV−vis; Cary-60) was used to record the absorption spectra of the polymers at wavelengths between 200 and 800 nm. Measurements were done using a quartz cuvette with a 1 cm path length at ca. 470−940 μM in a chloroform ($CHCl_3$) solvent.

2.3.2. Thermal Properties. Melting point apparatuses (SRS DigitMelt; Stanford Research Systems and Thermo MELT TEMP; Cole-Palmer) were used to record the melting temperature of the four new diacid and diol monomers. Thermalgravimetric analysis (TGA; Shimadzu TGA-50) was used to record weight loss of the FBP and SBP polymers between 25 and 800 °C in a nitrogen atmosphere at 10 °C/min. Initial sample weights were ∼8 mg. Differential scanning calorimetry (DSC; Netzsch Polyma 300) was used to evaluate the presence/absence of first-order (melting, T_m, and crystallization, T_c) and second-order thermal transitions (glass transition temperature, T_g) of the FBP and SBP polymers. 5−8 mg of each sample was hermetically sealed into aluminum pans. The temperature was cycled from 20 to 250 °C at 20 °C/min, except for polymer S2, which has a start temperature of 0 °C to accommodate for the low T_g. We report the second heating cycle for each polymer.

2.3.3. Molecular Weight. Size exclusion chromatography (SEC; Viscotek TriSEC-302) with three columns (Viskotek LT 3000L, T2500, T6000M) in a column oven and a differential refractometer, both maintained at 40 °C with a 1 mL/min flow rate, was used to record the molecular weights, M_n and M_w, and polydispersity, $Đ$. Polystyrene standards in THF were used to calibrate the SEC. Polymer solutions were prepared with HPLC-grade THF in 2−3 mg/mL concentrations and filtered through 0.2 μm filters before use.

2.3.4. Refractive Index. Variable-angle spectroscopic ellipsometry (J. A. Woollam M-2000 ellipsometer) was used to record the refractive index of polymer films on Si chips at room temperature. The polymer samples were prepared using the following protocols. 5 mL solutions were prepared in 1,2-dichloroethane at 3 wt/wt % concentration. The Si chips (∼1 cm^2) were cleaned by immersing in fresh Piranha, followed by rinsing with copious amounts of deionized water (DI H_2O) and isopropanol, and then drying under a dry nitrogen flow. (**CAUTION:** Piranha solution is a mixture of sulfuric acid and hydrogen peroxide. It is extremely oxidizing and reacts violently with organic matter. Proper precautions must be taken before, during, and after use.) The polymer solutions were spun coat on the clean Si chips at 500 rpm for 5 s and 850 rpm for 30 s using a spin coater (Laurell inc.). Two cleaned Si chips were treated with ozone (5−20 min; 15 mW/cm^2 at 185 nm; Ossilla) to improve polymer adhesion to the Si chip. Film thicknesses were measured using a profilometer (Bruker Dektak XT) and averaged 345 ± 15 nm.

2.3.5. Bioactivity of the T47D-KBLuc Cell Line. T47D-KBLuc cells were thawed from frozen stocks (CRL-2865, ATCC) and cultured in growth media (RPMI with 10% charcoal-stripped FBS (Atlanta Bio) and 1% HEPES (10 mM final concentration, Sigma)) on tissue culture flasks (BD Biocoat) at 37 °C in a humidified incubator (95% air, 5% CO_2). At 70−90% confluence, cells were trypsinized (0.25% trypsin/EDTA, Corning) and seeded into 96-well plates (∼50,000 cells/cm^2). Cells were allowed to adhere overnight and then were treated with monomers (0−100 μM) in growth media in the presence of estradiol (10 nM, Sigma-Aldrich) or in growth media alone for 24, 48, or 72 h. After the specified time points, cells were incubated with resazurin (TCI America) for 3 h to determine metabolic activity and then treated with Hoescht (33342, Invitrogen) to stain nuclei to allow for a cell count determination. Following imaging (Pico,

https://doi.org/10.1021/acsomega.4c10782
ACS Omega 2025, 10, 9613−9622

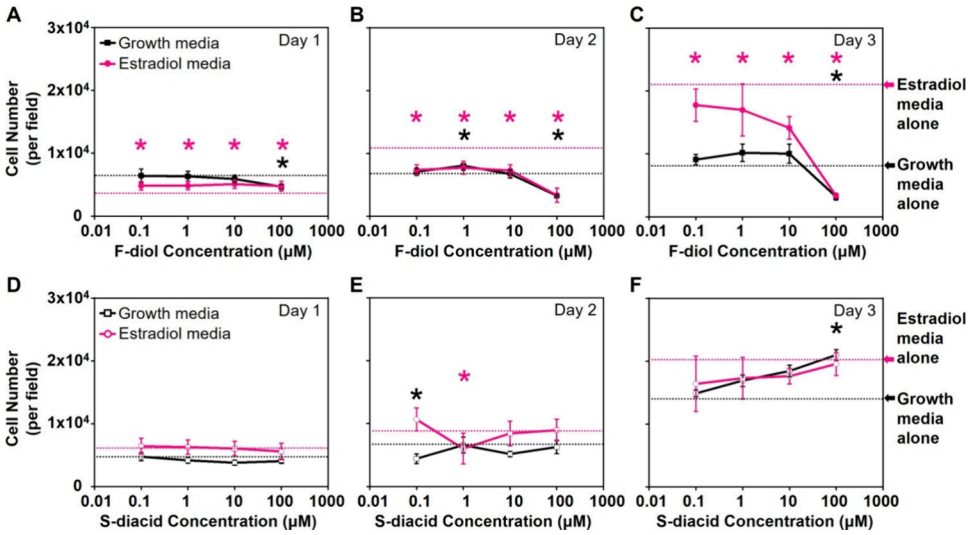

Figure 2. T47D-KBLuc cell response to increasing F-diol (A−C) or S-diacid (D−F) monomer concentrations. Dashed lines represent cell numbers without a monomer in growth media alone (black dashes) and estradiol media alone (pink dashes). Symbols with error bars represent the mean ± SD. The asterisks signify a statistically significant difference vs estradiol medial alone (pink *), or vs growth media alone (black *).

Molecular Devices), cells were rinsed with PBS and lysed (100 μL of 10 mM HEPES pH 7.4, freeze/thaw), and then the luciferase activity was assessed (GoldBio Luciferase Assay). Cells were automatically counted from the nuclear stain; each field was 3,462 μm^2 (CellReporterXpress, v2.9.3.1183, Molecular Devices). A two-way ANOVA was used (GraphPad Prism, v10.1.1) to analyze data (plotted as the mean ± S.D.), with media and monomer dose as the two factors. Dunnett's correction was used for the post hoc comparison of monomer dose vs media controls; an adjusted $p < 0.05$ was considered statistically significant.

3. RESULTS AND DISCUSSION

3.1. Monomer Structure and Properties. ^{1}H and ^{13}C NMR spectroscopies confirm the monomer structures; Figures S1−S4. The peak locations are consistent with predictions for monomer structures, F-diacid (Figure S1), S-diacid (Figure S2), F-diol (Figure S3), and S-diol (Figure S4). The m/z values resulting from GC-MS analysis match the theoretical molecular weights of the F-diol and S-diol monomers. The theoretical molecular weight of the F-diol is 438.51 g/mol with a parent peak GC-MS result of 438 m/z (Figure S5A). Similarly, the theoretical molecular weight of the S-diol is 338.35 g/mol with a parent peak GC-MS value of 338 m/z (Figure S5B). The parent peak m/z values for the diacids do not match their theoretical molecular weights but instead match fragments of the diacids. The differential is expected and is typical for carboxylic acids. Due to their high polarity, carboxylic acids can stick strongly to GC columns, resulting in fragmentation with parent peak m/z values different from the original polar compound.[35] The theoretical molecular weight for the F-diacid is 466.45 g/mol, whereas the m/z value is 494 m/z, a difference of about 28 (Figure S5C). Fragments adding up to 28 are common in MS and often comprise two carbons and four hydrogens or one carbon and one oxygen. The theoretical molecular weight for the S-diacid is 422.34 g/mol, whereas the m/z value is 306 m/z, a difference of ca. 116 (Figure S5D). The S-diacid starting material, SDMP, has a molecular weight of 306.30 g/mol, indicating fragmentation of the carboxylic acids, CH_2COO (58.02 g/mol), which adds to the 116 difference between the S-diacid molecular weight (422.34) and the GC-MS parent peak (306 m/z). Although not conducted with the F- and S-diacids in this work, fragmentation may be avoided by protecting the polar carboxylic acid groups via esterification, silylation, or a similar technique.[35] Representative product yields for the new F- and S-diacid precursors following the Williamson Ether reaction are 72 and 58%, respectively. Complete recovery of the F- and S-diacid monomers is common, following precursor hydrolysis. The synthesized monomers appear as solid powders with a white or beige color. The sulfone-containing monomers (S-diacid and S-diol) melt at higher temperatures than their fluorene-containing counterparts. For example, the T_m range for the F-diacid is 148−151 °C, but the S-diacid does not exhibit a T_m before the onset of yellowing at ca. 280 °C, indicating degradation (at which point melting characterization was stopped). The representative T_m range for the F-diol is 107−111 °C, while the S-diol exhibits a melting onset 70 degrees higher with a T_m range of 177−179 °C. The increase in T_m for the sulfone-containing monomers may result from better packing than the bulkier fluorene moiety. The characterization results for the F- and S-diols match previous reports.[34,36]

3.1.1. Monomer Bioactivity. F-diol and S-diacid monomers were evaluated for their impact on the T47D-KBLuc cell number and bioactivity at the estrogen receptor as a function of time and dose. Resource limitations for this work prevented evaluation of the other monomers. The F-diol displays time- and dose-dependent effects on cell viability and proliferation, with estradiol showing proliferative effects by day 3 vs growth media alone; Figure 2. Specifically, the F-diol-treated cells in estradiol media, at dose concentrations of 0.1, 1, 10, and 100 μM, exhibit significantly higher cell numbers on day 1 compared to the lower cell numbers on days 2 and 3; Figure 2A−C. Conversely, the S-diacid shows relatively little effect on cell viability and proliferation at dose concentrations below 100 μM. Specifically, the S-diacid-treated cells in growth and estradiol media at the same 0.1−100 μM dose concentrations show no difference in the cell number on day 1. On day 2, there is a growth depression at 0.1 μM and the cell count

https://doi.org/10.1021/acsomega.4c10782
ACS Omega 2025, 10, 9613−9622

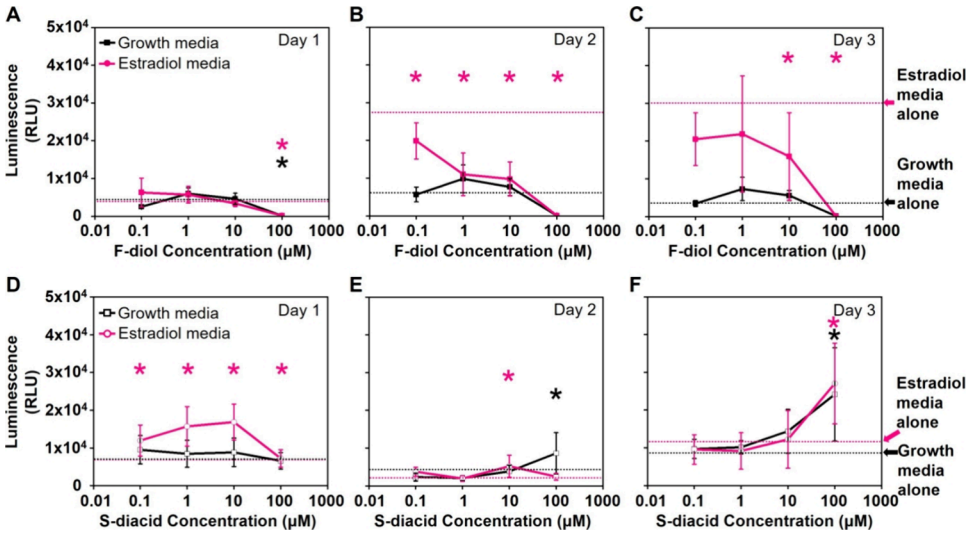

Figure 3. Estrogen-driven luminescence of cells treated with increasing F-diol (A−C) or S-diacid (D−F) monomer concentrations on day 1 (A and D), day 2 (B and E), and day 3 (C and F). The dashed lines represent luminescence in the absence of monomer in growth media alone (black dashes) or estradiol media alone (pink dashes). Symbols with error bars represent the mean ± SD. The asterisks signify a statistically significant difference vs estradiol media alone (pink *) or vs growth media alone (black *).

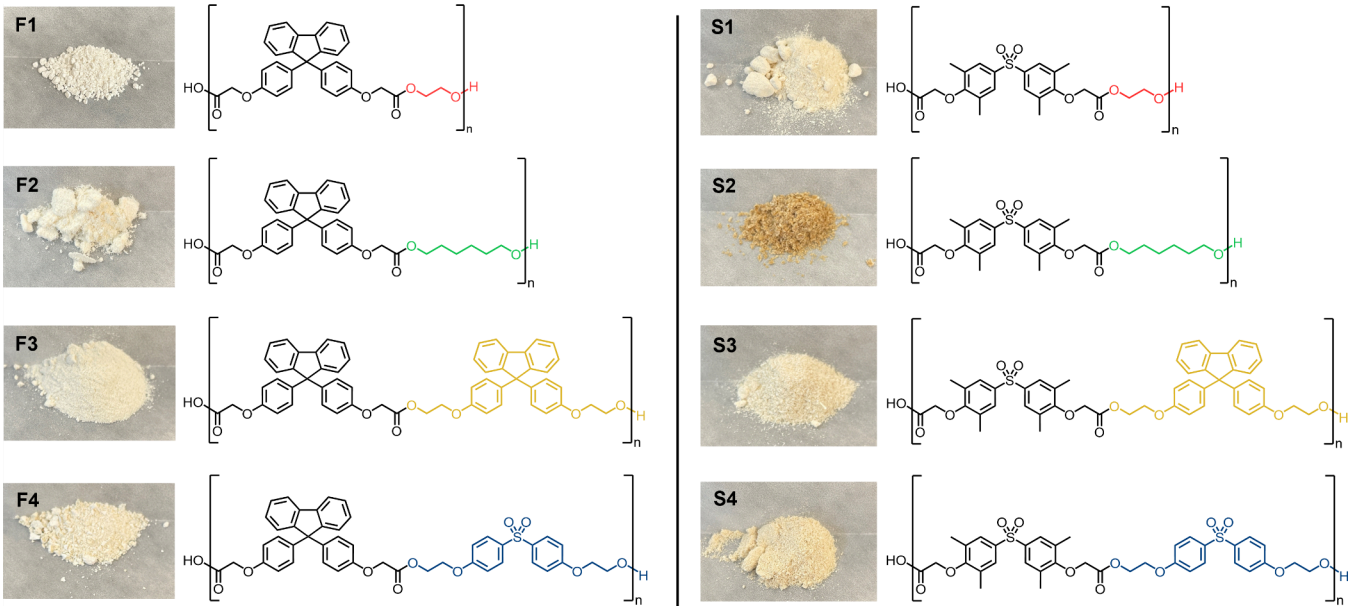

Figure 4. F1−4 and S1−4 polymer structures (NMR in the Supporting Information, Figures S7−S14), and optical image of typical FBP and SBP samples' appearance in the powder form.

decreases in estradiol media at 1 μM. Day 3 shows an apparent dose-dependent increase in cell number in both growth and estradiol media, becoming statistically significant at 100 μM in the growth media; Figure 2D−F.

In terms of activity at the estrogen receptor (Figure 3), F-diol displays an inhibitory effect in both the growth and estradiol-containing media (Figure 3A−C). This inhibition is most clearly seen on day 2; Figure 3B. Conversely, the S-diacid shows a significant increase in the estrogen response element-driven luciferase activity in the estradiol media on day 1, but the significant increase is largely absent in the following days except at 10 μM on day 2 and 100 μM on day 3. The S-diacid also shows a significant increase in the estrogen response element-driven luciferase activity in the growth media, but only at 100 μM on days 2 and 3; Figure 3D−F. Collectively, the cell effects of the monomers were significant for F-diol and S-diacid, albeit in different ways. F-diol exhibits clear cytotoxicity at the highest dose (100 μM) and an apparent inhibition of the estrogen response, i.e., antiestrogenic activity. The antiestrogenic effect of F-diol occurs for both suppressing the estrogen stimulation of growth and estrogen promoter-driven luminescence. S-diacid shows less significant effects on cell growth and viability but does seem to have a small dose-dependent impact on proliferation. If it were possible to normalize the luminescence to cell number, the significant increases observed in Figure 3D−F may become insignificant. There is also some potential that S-diacid interacts with the estradiol, making it more potent despite using estradiol at a concentration that seems to give maximal stimulation; Figure S6.

https://doi.org/10.1021/acsomega.4c10782
ACS Omega 2025, 10, 9613−9622

3.2. Polymerization. A driving motivation for the synthesis of F- and S-diacid compounds in this work is to establish if they can be used as monomers in step-growth polycondensation when independently combined with four known diols: ethylene glycol (EG), 1,6-hexanediol (HX), F-diol, and S-diol. ^{1}H and ^{13}C NMR spectroscopies confirm that both the F- and S-diacids successfully combine with EG, HX, F-diol, and S-diol monomers to form eight distinct polymer structures. The resulting polymer labels are F1−4 for the polymers containing the F-diacid with EG (F1), HX (F2), F-diol (F3), and S-diol (F4) and S1−4 for the polymers containing the S-diacid with EG (S1), HX (S2), F-diol (S3), and S-diol (S4). The average yield for the eight polymers is 82%, equating to ca. 1 g of material for characterization. The eight polymers are white or beige following precipitation in methanol (Figure 4). The average yield for the resulting polymers is 82%. The lower yield is significantly improved over earlier trials with 0−50% yields (not shown) but likely remains at less than 100% because of loss during precipitation in methanol as the filtrates were not transparent, indicating passage of some polymer through the filtration membrane. Further, the yield may be increased by reducing the deactivation of DIC from the formation of urea side-products by increasing the DPTS/DIC ratio and/or by changing the reaction temperature/time. Parallel results of the F-diol and S-diacid monomers on T47D-KBLuc cell counts and bioactivity at the estrogen receptor are factors in discontinuing attempts to further increase the yield (see Monomer Bioactivity above). Instead, the chemical and physical properties of the existing F1−4 and S1−4 polymers are described in the following sections.

3.2.1. Chemical Structure and Molecular Weight. ^{1}H and ^{13}C NMR spectroscopies confirm the structural formation of F1−4 and S1−4. NMR spectra with peak integration are shown in Figures S7−S14. ATR-FTIR analysis aids in identifying structural components like aromatic C=C (1590−1606 cm^{-1}), C−H (2861−3045 and 1451−1504 cm^{-1}), and C=O (1735−1757 cm^{-1}) stretches; Figure S15. SEC confirms the polymer's M_n, M_w, and $Đ$; Table 1. The M_w and $Đ$ are in the range of 17.0−53.4 kDa and 1.4−1.7 for F1−4 and 17.3−64.2 kDa and 1.6−3.9 for S1−4. The lower degrees of polymerization likely stem from incomplete monomer-to-polymer conversion because step-growth polymerization requires reaction completion to reach sufficiently larger chain lengths. The occasional presence of low-molecular-weight shoulders overlapping with the primary SEC peaks reflects incomplete conversion; Figure S16. For instance, representative samples of F3, S1, S3, and S4 display a secondary, low-molecular-weight peak (S1 and S4) or shoulders not fully resolvable from the primary response peak in SEC (F3 and S3). The lower M_w for some samples may stem from water contamination, a side product of the polymerizations. The $Đ$ values are lower than those anticipated for step-growth polymerization. Aside from incomplete polymerization, the moderate $Đ$ values could be from using polystyrene as standards for calibrating the SEC and the potential loss of lower-molecular-weight chains due to their solubility in a MeOH mixture during polymer precipitation.

Table 1. FBP and SBP Data: Molecular Weight (M_w), Dispersity ($Đ$), Glass Transition Temperature (T_g), and Temperature at 10% Sample Weight Loss ($T_{d\text{-}10\%}$)

	M_w (kDa)	$Đ$	T_g (°C)	$T_{d\text{-}10\%}$ (°C)	yield (%)
F1	18.0	1.4	93.4	350	93
F2	17.5	1.6	70.4	387	68
F3	20.5	1.7	112.9	374	83
F4	53.4	1.7	101.1	398	86
S1	64.2	3.9	78.4	358	77
S2	54.3	2.1	40.2	351	72
S3	30.9	1.7	116.5	386	84
S4	17.3	1.6	89.4	361	93

3.3. Material Properties. The FBP and SBP polymers were evaluated for their thermal and optical properties and solubility in a range of organic solvents using TGA, DSC, UV−vis, and ellipsometry. A brief consideration of the polymers' deteriorative properties was also evaluated. All eight polymers are readily soluble in chlorinated and nonpolar solvents (e.g., chloroform, hexane, and toluene) and some polar aprotic solvents (e.g., dimethyl sulfoxide). Their good solubility facilitated UV−vis sample preparation and polymer processing (spin coating) for optical characterization. Despite incomplete polymerization, the polymers have high degradation temperatures (ca. 350 °C) and are glassy (ca. 40−116 °C). They have high optical transparency in the visible region and high refractive indices. Chain degradation occurs under basic (pH 10.5) conditions and an elevated temperature (60 °C).

3.3.1. Thermal. Both the FBP and SBP polymers undergo similar two-step degradation patterns. In general, sample weights for F1−4 are stable until the beginning of the first degradation step at ca. 350 °C, except for F1, which begins gradually losing weight at ca. 170 °C prior to the first degradation step. 10% weight loss for the FBPs occurs at 350 °C for F1, 387 °C for F2, 374 °C for F3, and 398 °C for F4. FBP sample weights become relatively stable between 480 and 600 °C before beginning the second degradation step, wherein complete degradation occurs between 750 and 800 °C; Table 1 and Figure 5A.

Although the two-step degradation patterns are similar for the FBP and SBP samples, the SBPs undergo thermal degradation transitions at lower temperatures. For example, general sample weights for S1−4 are stable until the beginning

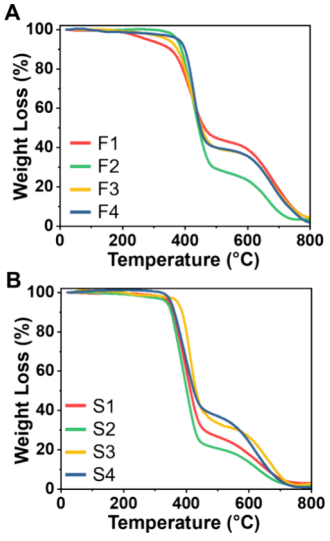

Figure 5. TGA of representative FBP and SBP. (A) Polymers F1−4. (B) Polymers S1−4.

https://doi.org/10.1021/acsomega.4c10782
ACS Omega 2025, 10, 9613−9622

of the first degradation step at ca. 340 °C (in comparison to 350 °C for F1−4), except for S3, which is the most thermally stable of the eight polymers, beginning the first degradation step at ca. 365 °C, nearly 15 °C higher than the FBPs and ca. 25 °C higher than its SBP counterparts (S1, S2, and S4). 10% weight loss for the SBPs occurs at 358 °C for S1, 351 °C for S2, 386 °C for S3, and 361 °C for S4. SBP sample weights become relatively stable between ca. 450−460 °C before beginning the second degradation step, wherein complete degradation occurs by ca. 750 °C for S1−4; Table 1 and Figure 5B. S3 is made using the bulky F-diol, which is a likely contributing factor in its overall greater thermal stability than the FBPs and remaining SBPs.

DSC characterization shows the FBP and SBP polymers are amorphous with T_g values ranging from ca. 40 to 116.5 °C with no detection of melting, T_m, or crystallization, T_c, transitions; Table 1. An important consideration when assessing transition temperatures is the Fox−Flory equation, which conveys a dependence of T_g on molecular weight at sufficiently low molecular weights, wherein the observed T_g will be lower than the material's glass transition temperature at infinite molecular weight, T_g^∞.[37] The molecular weight range of the polymers in this work ought to be considered as T_g at the prescribed molecular weight as opposed to the polymers' T_g^∞. This factor notwithstanding, the overall findings suggest that the fluorene derivatives restrict backbone flexibility more than the sulfonyl-phenylene derivatives, perhaps due to fluorene's steric bulk. For example, the molecular weights for the FBPs are, in general, smaller than for the SBPs (except for the case of F4, which is higher than its S4 counterpart), but their T_g values are higher. The T_g values for F1 and S1 are 93.4 and 78.4 °C, respectively. Similarly, F2 and S2 are 70.4 and 40.2 °C, F3 and S3 are 112.9 and 116.5 °C, and F4 and S4 are 101.1 and 89.4 °C, respectively; Figure 6. One consideration is the case of F3 in comparison to S3, whose T_g is 3.6 °C lower than that of S3. However, S3 contains fluorene and has a higher molecular weight than F3 (30.9 kDa for S3 vs 20.5 kDa for F3).

3.3.2. Optical. UV−vis spectroscopy demonstrates the light absorption characteristics of representative FBP and SBP samples in $CHCl_3$; Figures 7A,B and S17. F1−4 and S1−4 absorb only wavelengths between ca. 228 and 320 nm in the UV range. F1−4 exhibit four broad absorption peaks, each with decreasing molar absorptivity (ε, $M^{-1}\cdot cm^{-1}$) as a function of increasing wavelengths and a small shoulder with low ε at 228 nm. The λ_{max} for F1−4 ranges from 236 to 252 nm (ε = 771−1866 $M^{-1}\cdot cm^{-1}$), where F1 and F3 (with respective EG and F-diol monomers) are 236 nm, F2 (containing the HX diol monomer) is 237 nm, and F4 (containing the S-diol monomer) is 252 nm. The presence of the sulfonyl-phenylene functional group in the S-diol is the likely cause for the bathochromic shift of F4's λ_{max}, as the SBP samples exhibit λ_{max} at higher wavelengths and are the greatest when both the diacid and diol monomer units contain sulfonyl-phenylene functional groups. Furthermore, F4 has a broad shoulder around 264 nm and most closely resembles the absorption characteristics of S3, which is reasonable considering that the F4 and S3 polymers contain both fluorene and sulfonyl-phenylene functional groups. The second largest ε peak for F1−4 is broad with an apex at 275 nm, where the right side of the peaks has a slightly discernible shoulder at 287 nm. The third largest ε peak for F1−4 apexes at 310 nm and likely stems from the extended pi-conjugation of the fluorene functional group in F-diacid and F-diol monomers—the lowest ε peak for F1−4 apexes at 298 nm. The λ_{max} values for S1−4 range from 238 to 256 nm (ε = 600−2009 $M^{-1}\cdot cm^{-1}$), where S1 and S2 (containing the EG and HX monomers) have similar absorption characteristics, S4 (containing the S-diol monomer) somewhat resembles S1−2, and S3 (containing the F-diol monomer) is unique from S1−3. The λ_{max} is 253 nm for S1 and S2, 238 nm for S3, and 256 nm for S4. The ε for S4 is much lower (600 $M^{-1}\cdot cm^{-1}$) than for S1−2 (1900−2000 $M^{-1}\cdot cm^{-1}$) and has a more predominant left shoulder (236 nm for S4 and 234 nm for S1−2). There are slight shoulders to the right of λ_{max} at 281 nm for S1, S2, and S3 and at 274 nm for S1−2. The absorption characteristics for S3 are similar to F1−3 with lower λ_{max} (238 nm vs 236−237 nm) and minor peaks at higher wavelengths (287 and 310 nm). Similarities between

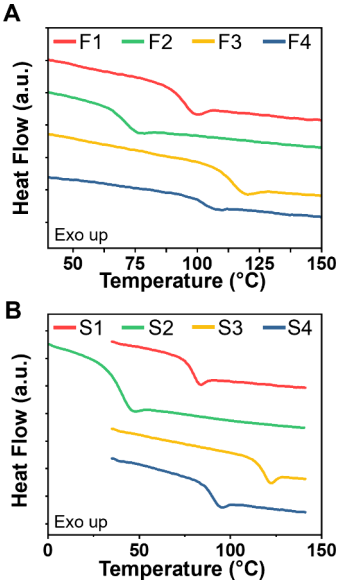

Figure 6. Normalized DSC curves of representative FBP and SBP. (A) Polymers F1−4. (B) Polymers S1−4.

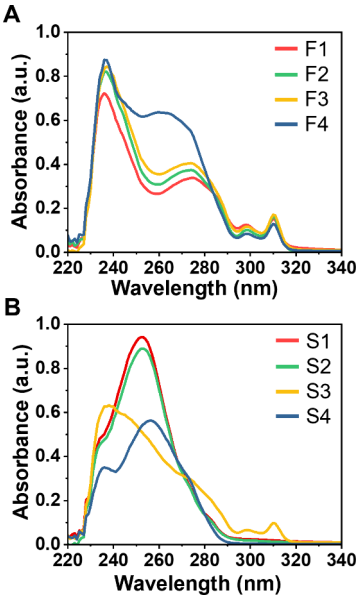

Figure 7. UV−vis of representative FBP and SBP samples in $CHCl_3$ at room temperature. (A) Polymers F1−4. (B) Polymers S1−4.

https://doi.org/10.1021/acsomega.4c10782
ACS Omega 2025, 10, 9613−9622

S3 and F1−3 are reasonable, considering that S3 contains a fluorene functional group akin to F1−3.

Ellipsometry demonstrates the interaction between incident light and thin films of representative FBP and SBP samples (refractive index, n). The F1−4 polymers have a higher average n (n = 1.63) than S1−4 (n = 1.58) across all visible wavelengths, as shown in Table 2. For example, at 587.56 nm,

Table 2. n_d, n_F, n_C, and Abe Number (V_d) for F1−4 and S1−4 Polymers

	n_d (587.6 nm)	n_F (486.1 nm)	n_C (656.3 nm)	V_e
F1	1.62	1.64	1.61	28.1
F2	1.60	1.62	1.59	25.0
F3	1.69	1.71	1.68	27.5
F4	1.63	1.65	1.62	24.2
S1	1.56	1.57	1.56	32.8
S2	1.56	1.58	1.56	28.1
S3	1.60	1.62	1.60	25.2
S4	1.59	1.61	1.59	29.6

a common wavelength for reporting refractive index, the n for F1−4 ranges from 1.60 to 1.69, where F1 = 1.62, F2 = 1.60, F3 = 1.69, and F4 = 1.63. However, the n for S1−4 at the same wavelength range from 1.56 to 1.60, where S1 = 1.56, S2 = 1.56, S3 = 1.60, and S4 = 1.59. The refractive index is the highest for F3 and S3 (1.69 and 1.60, respectively), which contain more fluorene monomer units than the other six polymers (remembering that F3 comprises both the F-diacid and the F-diol monomers, and S3 comprises the S-diacid alongside the F-diol). The n values for F3 and S3 are higher than those of the remaining polymers because of the greater incorporation of aromatic groups. The overall high n values for F1−4 and S1−4 stem from the aryl and sulfur groups. These moieties have high molar refractivity and low molar volume, which tend to increase a polymer's refractive index.[38−41] Another consideration in assessing interactions between light and polymer films, particularly in optical applications, is the Abbe number, V_d. The Abbe number provides classification values of glassy materials in terms of their chromaticity—the quality of color. V_d is calculated according to eq 1

$$V_d = \frac{n_d - 1}{n_F - n_C} \quad (1)$$

where n_d, n_F, and n_C are refractive index values at the Fraunhofer d, F, and C spectral lines (587.56, 486.1, and 656.3 nm, respectively).[42,43] V_d values for the FBP and SBP materials in this work are low, ranging from 24.2 to 32.8; Table 2 (Table 2 also provides n_d, n_F, and n_C). We anticipate lower values because of the high n for F1−4 and S1−4.[38] For comparison, V_d for polycarbonates, a common lens material with some structural similarity, is ca. 34.[44] Further, the V_d values for fluorene and sulfone moieties typically range from ca. 30 to 50.[45,46]

4. CONCLUSIONS

We report eight new FBP and SBP polyesters, F1−4 and S1−4, from two new monomers, 2,2′-(((9*H*-fluorene-9,9-diyl)bis(4,1-phenylene))bis(oxy))diacetic acid (F-diacid) and 2,2′-((sulfonylbis(2,6-dimethyl-4,1-phenylene))bis(oxy))diacetic acid (S-diacid). We demonstrate the step-growth polymerization feasibility of the new diacid monomers by pairing individually with four different diols, ethylene glycol (EG), 1,6-hexanediol (HX), 2,2′-(((9*H*-fluorene-9,9-diyl)bis(4,1-phenylene))bis(ethan-1-ol) (F-diol), and 2,2′-((sulfonylbis-(4,1-phenylene))bis(oxy))bis(ethan-1-ol) (S-diol). By varying the diol counterpart with the new F-diacid and S-diacid monomers, we demonstrate the tunability of their glass transition temperature, T_g, and the feasibility of polymerization with monomers encompassing different steric bulk (lower for EG and HX, and higher for F-diol and S-diol). Diacid monomer yields are ≥58%. Polymer yields average 82%. M_w values range from 17.3 to 77 kDa with an average $Đ$ of 1.5. The SEC of some samples exhibits a second small low-molecular-weight peak or shoulder, suggesting incomplete polymerization in those cases, which coincides with the moderate yields. All new polyesters, F1−4 and S1−4, absorb light in the UV range, with no absorption in the visible range; they display high refractive indices, averaging n = 1.63 for F1−4 and n = 1.58 for S1−4, with low Abbe numbers ranging from 24.2 to 32.8. The cardo polymers reported in this work have the potential to depolymerize through base-supported hydrolysis of ester linkages. Our lab is conducting a comprehensive analysis of the current materials' depolymerization kinetics and structural products following exposure to different environmental stressors, which we plan to report on in due course. Finally, the F-diol monomer exhibits antiestrogenic activity and is cytotoxic at 100 μM doses against the T47D-KBLuc cell line in both growth and estradiol-containing media. The S-diacid monomer has some interaction with estradiol, making the estradiol potentially more potent, which is undesirable bioactivity. The negative bioactivity from both the F-diol and the S-diacid occurred despite extending end groups on either side of the fluorene and sulfone, respectively, which was done in an attempt to mitigate the estrogenic bioactivity observed in traditional fluorene and sulfone monomers, such as BPF, BHPF, and BPS. Estrogenic bioactivity can lead to developmental malformations, interfere with reproduction, and increase cancer risk, among other disturbances. Thus, results from these cell-line studies highlight the growing need to comprehend the biological impacts of newly developed materials, in addition to their conventional chemical and material properties.

■ ASSOCIATED CONTENT

Data Availability Statement

The data supporting this article have been included as part of the Supporting Information.

Supporting Information

The Supporting Information is available free of charge at https://pubs.acs.org/doi/10.1021/acsomega.4c10782.

Synthetic details, NMR, ATR-FTIR, SEC, UV−vis, T47D-KBLuc's dose-dependent response to estradiol, and preliminary degradation data (PDF)

■ AUTHOR INFORMATION

Corresponding Authors

Thomas J. Kean − *Biionix Cluster, University of Central Florida, Orlando, Florida 32827, United States; College of Medicine, University of Central Florida, Orlando, Florida 32826, United States;* orcid.org/0000-0001-6844-3404; Email: thomas.kean@ucf.edu

Kaitlyn E. Crawford − *Department of Materials Science and Engineering and NanoScience Technology Center, University of Central Florida, Orlando, Florida 32826, United States;*

https://doi.org/10.1021/acsomega.4c10782
ACS Omega 2025, 10, 9613−9622

Biionix Cluster, University of Central Florida, Orlando, Florida 32827, United States; Department of Chemistry, University of Central Florida, Orlando, Florida 32816, United States; orcid.org/0000-0001-7396-6349; Email: kcrawford@ucf.edu

Authors

Gavin S. Mohammad-Pour − *Department of Materials Science and Engineering, University of Central Florida, Orlando, Florida 32826, United States; Biionix Cluster, University of Central Florida, Orlando, Florida 32827, United States; 280 Earth, Palo Altro, California 94303, United States;* orcid.org/0000-0002-3157-8644

Aditya Maan − *Department of Materials Science and Engineering, University of Central Florida, Orlando, Florida 32826, United States; Biionix Cluster, University of Central Florida, Orlando, Florida 32827, United States*

Rachel Kemp − *College of Medicine, University of Central Florida, Orlando, Florida 32826, United States*

Complete contact information is available at: https://pubs.acs.org/10.1021/acsomega.4c10782

Author Contributions

G.S.M.-P.: Project development, monomer and polymer synthesis and characterization, and manuscript editing. A.M.: Monomer synthesis and characterization, polymer characterization, and manuscript writing and editing. R.K.: Monomer bioactivity testing. T.K.: Monomer bioactivity analysis and manuscript writing. K.E.C.: Project development and oversight, polymer data interpretation, and manuscript writing. All authors approved the contents of this manuscript. G.S.M.-P. and A.M. contributed equally to this work.

Notes

The authors declare no competing financial interest.

■ ACKNOWLEDGMENTS

The authors would like to acknowledge the postdoctoral preeminence fellowship provided by the University of Central Florida's Office of Research. Article processing charges were provided in part by the UCF College of Graduate Studies Open Access Publishing Fund.

■ REFERENCES

(1) Ramsdale, C. M.; Greenham, N. C. Ellipsometric Determination of Anisotropic Optical Constants in Electroluminescent Conjugated Polymers. *Adv. Mater.* **2002**, *14* (3), 212−215.

(2) Shi, Y.; Wang, W.; Lin, W.; Olson, D. J.; Bechtel, J. H. Double-End Crosslinked Electro-Optic Polymer Modulators with High Optical Power Handling Capability. *Appl. Phys. Lett.* **1997**, *70* (11), 1342−1344.

(3) Qi, P.; Vermesh, O.; Grecu, M.; Javey, A.; Wang, Q.; Dai, H.; Peng, S.; Cho, K. J. Toward Large Arrays of Multiplex Functionalized Carbon Nanotube Sensors for Highly Sensitive and Selective Molecular Detection. *Nano Lett.* **2003**, *3* (3), 347−351.

(4) Hreha, R. D.; Haldi, A.; Domercq, B.; Barlow, S.; Kippelen, B.; Marder, S. R. Synthesis of Acrylate and Norbornene Polymers with Pendant 2,7-Bis(Diarylamino)Fluorene Hole-Transport Groups. *Tetrahedron.* **2004**, *60* (34), 7169−7176.

(5) Vallejos, S.; Estévez, P.; García, F. C.; Serna, F.; De La Peña, J. L.; García, J. M. Putting to Work Organic Sensing Molecules in Aqueous Media: Fluorene Derivative-Containing Polymers as Sensory Materials for The Colorimetric Sensing of Cyanide In Water. *Chem. Commun.* **2010**, *46* (42), 7951.

(6) Choi, J.; Lee, K. M.; Wycisk, R.; Pintauro, P. N.; Mather, P. T. Nanofiber Network Ion-Exchange Membranes. *Macromolecules* **2008**, *41* (13), 4569−4572.

(7) Ward, J.; Simmons, R.; Chatam, P. Internal Anti-Static Agents for Engineering Plastics. *Annu. Technol. Conf.-Soc. Plast. Eng.* **1998**, *2* (52), 1782−1786.

(8) Watanabe, T.; Sano, T.; Ito, H. Antistatic Properties of Transparent Plastics Using a Donor-Accepter Molecular Compound Antistatic Agent. *J. Polym. Eng.* **2018**, *38* (6), 555−561.

(9) Chong, H.; Nie, C.; Zhu, C.; Yang, Q.; Liu, L.; Lv, F.; Wang, S. Conjugated Polymer Nanoparticles for Light-Activated Anticancer and Antibacterial Activity with Imaging Capability. *Langmuir* **2012**, *28* (4), 2091−2098.

(10) Shintani, H.; Suzuki, E.; Sakurai, M. Determination of Compounds Inhibiting Bacterial Growth in Sterilized Medical Devices. *Chromatographia* **2003**, *58* (3−4), 193−199.

(11) Abbel, R.; Schenning, A. P. H. J.; Meijer, E. W. Fluorene-Based Materials and Their Supramolecular Properties. *J. Polym. Sci., Part A: Polym. Chem.* **2009**, *47* (17), 4215−4233.

(12) Watanabe, S.; Takayama, T.; Nishio, H.; Matsushima, K.; Tanaka, Y.; Saito, S.; Sun, Y.; Oyaizu, K. Synthesis Of Colorless and High-Refractive-Index Sulfoxide-Containing Polymers by The Oxidation of Poly(Phenylene Sulfide) Derivatives. *Polym. Chem.* **2022**, *13* (12), 1705−1711.

(13) Okutsu, R.; Suzuki, Y.; Ando, S.; Ueda, M. Poly(thioether sulfone) with High Refractive Index and High Abbe's Number. *Macromolecules* **2008**, *41* (16), 6165−6168.

(14) Chong, H.; Duan, X.; Yang, Q.; Liu, L.; Wang, S. Synthesis and Characterization of Degradable Water-Soluble Fluorescent Polymers. *Macromolecules* **2010**, *43* (24), 10196−10200.

(15) Guan, X.-H.; Nie, H.-R.; Wang, H.-H.; Zhao, J.-Y.; Wang, Z.-P.; Wang, R.; Liu, B.-F.; Zhou, G.-Y.; Gu, Q. High-Solubility Aromatic Polyesters With Fluorene and Phthalein Groups: Synthesis and Property. *High Perform. Polym.* **2020**, *32* (8), 933−944.

(16) Chamkure, Y. K.; Sharma, R. K. New organosoluble polyarylates containing pendent Fluorene units: synthesis, characterization and thermal behaviour. *J. Polym. Res.* **2019**, *26* (1), 17.

(17) Seesukphronrarak, S.; Kawasaki, S.; Kuwata, S.; Takata, T. Synthesis and characterization of 9,9-bis(4-hydroxyphenyl and 4-aminophenyl)dibenzofluorenes: Novel Fluorene-based monomers. *J. Polym. Sci., Part A: Polym. Chem.* **2019**, *57* (24), 2602−2605.

(18) Meng, S.; Sun, N.; Su, K.; Zhao, X.; Wang, D.; Zhou, H.; Chen, C. Novel Organosoluble Polyarylates based on Diphenylamine-Fluorene Units: Synthesis, Electrochromic, and Electrofluorescent Properties. *High Perform. Polym.* **2018**, *30* (7), 864−871.

(19) Bhole, Y.; Kharul, U. Effect of Fluorene-Bisphenol Ring Substitution and Bridge Rigidity on Physical and Gas Permeation Properties of Resulting Polyarylates. *Polym. Int.* **2003**, *52* (9), 1474−1479.

(20) Oishi, Y.; Harada, S.; Kakimoto, M.-A.; Imai, Y. Preparation and Properties of Fluorine-Containing Polyarylates from Tetrafluoroterephthaloyl Chloride and Bisphenols. *J. Polym. Sci., Part A: Polym. Chem.* **1989**, *27* (4), 1425−1428.

(21) Abel, S. B.; Frontera, E.; Acevedo, D.; Barbero, C. A. Functionalization of Conductive Polymers through Covalent Post-modification. *Polymers* **2023**, *15* (1), 205.

(22) Li, N.; Shin, D.-W.; Hwang, D.-S.; Lee, Y.-M.; Guiver, M. D. Polymer Electrolyte Membranes Derived from New Sulfone Monomers with Pendent Sulfonic Acid Groups. *Macromol.* **2010**, *43*, 9810−9820.

(23) Al-Azzawi, A. G. S.; Aziz, S. B.; Dannoun, E. M. A.; Iraqi, A.; Nofal, M. M.; Murad, A. R.; Hussein, M. A. A Mini Review on the Development of Conjugated Polymers: Steps towards the Commercialization of Organic Solar Cells. *Polymers* **2022**, *15* (1), 164.

(24) Shukla, A. K.; Alam, J.; Alhoshan, M. Recent Advancements in Polyphenylsulfone Membrane Modification Methods for Separation Applications. *Membranes.* **2022**, *12* (2), 247.

(25) Rochester, J. R.; Bolden, A. L. Bisphenol S and F: A Systematic Review and Comparison of the Hormonal Activity of Bisphenol A Substitutes. *Environ. Health Perspect.* **2015**, *123* (7), 643−650.
(26) Zhang, Z.; Hu, Y.; Guo, J.; Yu, T.; Sun, L.; Xiao, X.; Zhu, D.; Nakanishi, T.; Hiromori, Y.; Li, J.; et al. Fluorene-9-Bisphenol is Anti-Oestrogenic and May Cause Adverse Pregnancy Outcomes in Mice. *Nat. Commun.* **2017**, *8* (1), 14585.
(27) Yang, L.; Guo, X.; Mao, X.; Jia, X.; Zhou, Y.; Hu, Y.; Sun, L.; Guo, J.; Xiao, H.; Zhang, Z. Hepatic toxicity of Fluorene-9-bisphenol (BHPF) on CD-1 Mice. *Ecotoxicol. Environ. Saf.* **2021**, *219*, No. 112298.
(28) Jiao, X.; Ding, Z.; Meng, F.; Zhang, X.; Wang, Y.; Chen, F.; Duan, Z.; Wu, D.; Zhang, S.; Miao, Y.; et al. The Toxic Effects of Fluorene-9-Bisphenol on Porcine Oocyte In Vitro Maturation. *Environ. Toxicol.* **2020**, *35* (2), 152−158.
(29) Ciocca, D. R.; Roig, L. M. Estrogen Receptors in Human Nontarget Tissues: Biological and Clinical Implications. *Endocr. Rev.* **1995**, *16* (1), 35−62.
(30) Levin, E. R. Integration of the Extranuclear and Nuclear Actions of Estrogen. *Mol. Endocrinol.* **2005**, *19* (8), 1951−1959.
(31) Wilson, V. S.; Bobseine, K.; Earl Gray, L. J. Development and Characterization of a Cell Line that Stably Expresses an Estrogen-Responsive Luciferase Reporter for the Detection of Estrogen Receptor Agonist and Antagonists. *Toxicol. Sci.* **2004**, *81* (1), 69−77.
(32) Nakazawa, H.; Yamaguchi, A.; Inoue, K.; Yamazaki, T.; Kato, K.; Yoshimura, Y.; Makino, T. In Vitro Assay of Hydrolysis and Chlorohydroxy Derivatives of Bisphenol A Diglycidyl Ether for Estrogenic Activity. *Food Chem. Toxicol.* **2002**, *40* (12), 1827−1832.
(33) Papava, G. S. Synthesis and Study of Diols Containing Bisphenol Fragments and of Polymers Produced on Their Basis. *Acta Polym.* **1988**, *39* (8), 445−448.
(34) Türel Erbay, B.; Serhatlı, I. E. Synthesis of bis[(4-hydroxyethoxy)phenyl]sulfone containing urethane acrylates and their applications. *Progress in Organic Coatings* **2013**, *76* (1), 1−10.
(35) Pietrogrande, M.-C.; Bacco, D.; Mercuriali, M. GC-MS Analysis of Low-Molecular-Weight Dicarboxylic Acids in Atmospheric Aerosol: Comparison Between Silylation and Esterification Derivatization Procedures. *Anal. Bioanal. Chem.* **2010**, *396*, 877−885.
(36) Shang, Z.; Feng, M.; Jiang, M.; Zhang, Z.; Liu, S.; Wang, S.; Xu, F. Synergistic Catalysts of Lewis Acid and Brønsted Acid for Highly Efficient Preparation of Bisphenol Compounds. *Industrial & Engineering Chemistry Research* **2024**, *63* (8), 3576−3585.
(37) Fox, T. G.; Loshaek, S. Influence of Molecular Weight and Degree of Crosslinking on the Specific Volume and Glass Temperature of Polymers. *J. Polym. Sci.* **1955**, *15* (80), 371−390.
(38) Liu, J.-G.; Ueda, M. High Refractive Index Polymers: Fundamental Research and Practical Applications. *J. Mater. Chem.* **2009**, *19*, 8907−8919.
(39) Lorentz, H. A. Ueber die Beziehung zwischen der Fortpflanzungsgeschwindigkeit des Lichtes und der Körperdichte. *Annalen der Physik und Chemie* **1880**, *245* (4), 641−665.
(40) Lorenz, L. Ueber die Refractionsconstante. *Annalen der Physik und Chemie* **1880**, *247* (9), 70−103.
(41) Nakabayashi, K.; Sobu, S.; Kosuge, Y.; Mori, H. Synthesis And Nanoimprinting of High Refractive Index And Highly Transparent Polythioethers Based on Thiol-Ene Click Chemistry. *J. Polym. Sci., Part A: Polym. Chem.* **2018**, *56* (19), 2175−2182.
(42) Nakabayashi, K.; Imai, T.; Fu, M.-C.; Ando, S.; Higashihara, T.; Ueda, M. Poly(phenylene thioether)s with Fluorene-Based Cardo Structure toward High Transparency, High Refractive Index, and Low Birefringence. *Macromolecules* **2016**, *49* (16), 5849−5856.
(43) Bach, H.; Neuroth, N. *The Properties of Optical Glass*; Springer, 1998.
(44) Suri, G.; Jha, G. S.; Seshadri, G.; Khandal, R. K. Modification of Low Refractive Index Polycarbonate for High Refractive Index Applications. *Inter. J. Polym. Sci.* **2009**, *2009*, 1−8.
(45) Jang, J. Y.; Do, J. Y. Refractive Index Changes In Polyacrylates Bearing Alkyl Sulfur Groups Through The Sulfur Oxidation Reaction. *React. Funct. Polym.* **2015**, *91*−*92*, 28−34.
(46) Suzuki, Y.; Higashihara, T.; Ando, S.; Ueda, M. Synthesis of Amorphous Copoly(Thioether Sulfone)s With High Refractive Indices and High Abbe Numbers. *Eur. Polym. J.* **2010**, *46* (1), 34−41.

https://doi.org/10.1021/acsomega.4c10782
ACS Omega 2025, 10, 9613−9622